

Empirically-Driven Multiwavelength K-corrections At Low Redshift

Catherine E. Fielder,^{1,2*} Brett H. Andrews,^{2,3} Jeffrey Newman,^{2,3} Samir Salim⁴

¹*Steward Observatory, University of Arizona, Tucson, AZ, 85721, USA*

²*Department of Physics and Astronomy, University of Pittsburgh, Pittsburgh, PA 15260, USA*

³*Pittsburgh Particle Physics, Astrophysics, and Cosmology Center (PITT PACC), University of Pittsburgh, Pittsburgh, PA 15260, USA*

⁴*Department of Astronomy, Indiana University, Bloomington, IN, 47405, USA*

Accepted XXX. Received YYY; in original form ZZZ

ABSTRACT

K-corrections, conversions between flux in observed bands to flux in rest-frame bands, are critical for comparing galaxies at various redshifts. These corrections often rely on fits to empirical or theoretical spectral energy distribution (SED) templates of galaxies. However, the templates limit reliable *K*-corrections to regimes where SED models are robust. For instance, the templates are not well-constrained in some bands (e.g., WISE W4), which results in ill-determined *K*-corrections for these bands. We address this shortcoming by developing an empirically-driven approach to *K*-corrections as a means to mitigate dependence on SED templates. We perform a polynomial fit for the *K*-correction as a function of a galaxy’s rest-frame colour determined in well-constrained bands (e.g., $^{0}(g-r)$) and redshift, exploiting the fact that galaxy SEDs can be described as a one parameter family at low redshift ($0.01 < z < 0.09$). For bands well-constrained by SED templates, our empirically-driven *K*-corrections are comparable to the SED fitting method of KCORRECT and SED template fitting employed in the GSWLC-M2 catalogue (the updated medium-deep GALEX–SDSS–WISE Legacy Catalogue). However, our method dramatically outperforms the available SED fitting *K*-corrections for WISE W4. Our method also mitigates incorrect template assumptions and enforces the *K*-correction to be 0 at $z = 0$. Our *K*-corrected photometry and code are publicly available.

Key words: galaxies: photometry – galaxies: general – methods: data analysis – techniques: photometric

1 INTRODUCTION

Broad-band luminosity measurements are critical for understanding galaxy evolution, but require correcting for the redshifting of light across photometric band passes. The redshifting of a galaxy spectrum is equivalent to shifting the filter transmission curve through which the galaxy is observed. Hence two galaxies with identical rest-frame spectral energy distributions (SEDs) but at different redshifts will generally have different fluxes in the same observed band pass. This difference is referred to as the *K*-correction (Humason et al. 1956; Oke & Sandage 1968). *K*-corrections are especially important for comparing populations of galaxies at varying redshift, as we want equivalent measurements of the SEDs of these galaxies at all z . *K*-corrections serve as a critical equaliser, enabling practical comparisons amongst galaxy surveys at different redshift ranges.

For objects where the entire spectrum has been observed, *K*-corrections are straightforward to calculate, as the spectrum can be shifted to accommodate redshift corrections. However, the spectra obtained are frequently limited to the central region of a galaxy, so the appropriate *K*-correction for integrated photometry will likely differ. Since spectroscopy with full spatial coverage (or, better yet, spatially-resolved spectroscopy) is rarely available for large survey samples, we must depend on photometric information to derive *K*-corrections. In this paper, we develop new methods that can be used to derive *K*-corrections based upon photometric measurements, even when we

lack not only observed spectral measurements but even theoretical template spectra that may be used to guide predictions.

In order to determine the intrinsic brightness of an object in some rest-frame passband we use a transformation that acts upon the observed-frame photometry. The *K*-correction between a band-pass R used to observe a galaxy at redshift z and rest bandpass Q may then be defined by the equation (Oke & Sandage 1968; Hogg et al. 2002; Blanton & Roweis 2007)

$$M_Q = m_R - DM(z) - K_{QR}(z) + 5 \log h, \quad (1)$$

where M_Q is the absolute magnitude in the desired rest-frame passband Q , m_R is the observed apparent magnitude in passband R , $DM(z)$ is the distance modulus derived assuming a Hubble parameter $H_0 = 100$ km/s/Mpc, $K_{QR}(z)$ is the *K*-correction between band R and band Q , and h is the adopted value of the Hubble parameter divided by 100 km/s/Mpc. The distance modulus is defined as $DM(z) = 5 \log \left(\frac{d_L}{10 \text{ pc}} \right)$ where d_L is the luminosity distance. For brevity we do not include the full and rigorous formalism for the generalised definition of the *K*-correction, which is presented in Hogg et al. (2002) (see in particular Equations 8 and 10).

The key ingredients generally used to determine *K*-corrections for a given galaxy are (1) some knowledge of the spectrum of the object, which characterises the flux emitted by the galaxy across a large wavelength range, as well as (2) the response curves of the instrument used to make the observations, as the transmission function of different filters, the QE of different detectors, etc. will affect the collected photons slightly differently. Often we do not have much information

* E-mail: cfielder@arizona.edu

on the full spectrum of the objects we observe; instead, we merely have a handful of photometric points that sample various parts of the observed spectrum. This requires us to either use analytical approximations to quantify how the observed galaxy's colour changed with redshift, or to utilise templates to reconstruct the observed galaxy's rest-frame SED.

Historically, template matching has been the most commonly used approach. There are two families of SED templates that are used in this matching to determine K -corrections: empirical templates derived from a representative set of real galaxy spectra (e.g., Coleman et al. 1980; Kinney et al. 1996; Brown et al. 2014), or synthetic templates derived from stellar population synthesis (SPS) models (e.g., Bruzual & Charlot 2003; Maraston 2005). SPS models employ assumptions about the star formation and evolution within a galaxy and libraries of stellar spectra to construct a realistic SED. As a result SPS templates have the benefit of providing estimates of other physical quantities such as stellar mass, star formation rate, or dust attenuation in addition to K -corrected photometry.

There are a number of methods which have been used to calculate galaxy K -corrections in the literature. We briefly review K -correction methods here, but this list is not exhaustive. We then discuss the caveats to using these methods.

Early papers modelled K -corrections as a simple function of redshift and galaxy morphological type, such as in the work by Coleman et al. (1980). The authors used empirical SED templates for four morphological galaxy types (E, Sbc, Scd and Irr galaxies) to obtain K -corrections using the best data available at the time. However, this method is somewhat oversimplified based on our current understanding of galaxy evolution, as galaxies that may share the same morphology can have a diverse range of spectral properties (see, e.g., Uzeirbegovic et al. 2022).

It is more common to obtain K -corrections by modelling galaxy SEDs as a function of wavelength. This process begins by identifying a template rest-frame SED that matches the observed colours of a galaxy when shifted to that galaxy's redshift. The template may then be used to derive K -corrections and determine the rest-frame properties of the galaxy of interest. Maximum likelihood fitting of photometry to theoretical SPS-based SED models has often been utilised to calculate K -corrections such as in work by e.g., Bell et al. (2004) and Brown et al. (2007). As mentioned above, SPS models can provide reasonable approximations of real galaxy SEDs within the wavelength range of the spectral libraries used. However, while this method works very well for intrinsically red galaxies, the rest-frame spectra of blue galaxies are not as tightly constrained by broad-band photometry due to the effects of star formation, dust attenuation, and nebular emission lines which may have degenerate impacts on galaxy SEDs within the optical wavelength range but different impacts at shorter or longer λ . Even worse, existing SPS models may struggle to capture the full diversity of galaxy SEDs. Blanton et al. (2003) introduced K -correction calculations derived from matching photometric observations to templates constructed from combinations of Bruzual & Charlot (2003) SPS models, dust attenuation models, and nebular emission lines, which resulted in more realistic SEDs. This was the first instance of using multiple components to construct galaxy SEDs, which has served as the backbone of the commonly used KCORRECT software of Blanton & Roweis (2007) (now in version 4.3). KCORRECT has become a widespread standard for determining K -corrections and will serve as a comparison for our own results.

K -corrections have also been estimated using analytical functions of redshift which are parameterised in terms of some additional property that characterises the galaxy, separating out objects of different rest-frame SEDs. Willmer et al. (2006) fit second-order polynomi-

als to determine K -corrections as a function of a single **observed** colour and redshift, based upon the Kinney et al. (1996) empirical templates. This work was based upon photometry in only three bands (the CFHT 12K *BRI* filters used for DEEP2, the Deep Evolutionary Exploratory Probe; Newman et al. 2013) and used filters for which KCORRECT had not yet been tuned and tested (the fitting methods employed by Blanton et al. (2003) were not available) resulting in the need to develop other methods. Chilingarian et al. (2010) empirically showed that K -corrections can be effectively approximated as solely a function of redshift and a single colour, using 190,275 observed galaxies spanning the redshift range $0.03 < z < 0.6$. The authors derived K -corrections defined by polynomials that are fifth order in observed $(g - r)$ colour and third order in redshift for nine filters (*ugrizYJHK*), based upon both KCORRECT and PEGASE.2 (Fioc & Rocca-Volmerange 1997) SPS models. Work by O'Mill et al. (2011) took a similar approach, deriving a linear relationship between the K -correction, $(g - r)$ colour, and redshift for a number of galaxies of SDSS DR7 that were processed by KCORRECT v4.3. Beare et al. (2014) did a more in-depth study to determine which observed colours best characterise K -corrections for each SDSS optical band (*ugriz*), deriving second order polynomials in colour from the 129 empirical SEDs in the Brown et al. (2014) Atlas.

While K -corrections often can be determined accurately using template fits, there are also limitations to this approach. First, analyses generally employ only a limited number of template SEDs (or linear combinations thereof). As a result, the templates used may not span the full range of possible SEDs exhibited by a diverse galaxy sample. This is especially concerning for galaxies that have less commonplace SEDs, which could result in inaccurate K -corrections due to template mismatches. Second, although empirical templates may provide a better match to the SEDs of actual galaxies than model-based ones, the existing empirical template libraries only have limited wavelength coverage, particularly in the infrared, limiting their use. Additionally, many of the older commonly used empirical templates such as those from Coleman et al. (1980) and Kinney et al. (1996) are derived from galaxies with significant light from active galactic nuclei (AGN). This can lead to systematic errors due to the strong emission lines and blue continuum from the AGN outshining the stellar continuum. This problem is exacerbated for empirical templates that are based on the spectra of the centres of bright galaxies. Willmer et al. (2006) found that the use of such templates (for instance, several of the Kinney et al. 1996 templates) resulted in derived colours that are too red by 0.08 magnitudes. Empirical templates are also still limited by the small sets of galaxies for which robust observations over a broad wavelength range have been obtained, meaning some galaxy families do not have well-observed template SEDs. Theoretical SEDs may also cover a limited wavelength range for the same reason. Methods that employ model-based templates are also limited by the quality of the models used.

Regardless of which family of template is used, depending on them restricts our ability to determine K -corrections at wavelengths where the templates are not available, poorly constrained, or models are lacking. For example, the WISE bands probe the interstellar dust content of galaxies due to their sensitivity to polycyclic aromatic hydrocarbon emission features, the small-grain dust continuum, and the thermal emission tail of larger dust grains (Wright et al. 2010), which makes them important for studying a galaxy's characteristics. There are currently few options available for determining WISE K -corrections apart from KCORRECT. However, while KCORRECT will calculate K -corrections for the WISE photometric bands, these fits employ templates that do *not* include dust emission features, which are increasingly important for the longer-wavelength WISE bands

(W2 through W4). The absence of this feature in the templates should result in incorrect K -corrections.

In this work we have developed a data-driven approach to determining K -corrections that limits the extent to which templates are relied upon and that circumvents entirely the need for templates in filters where the SED is poorly known. Conceptually, our method builds on the work of Willmer et al. (2006), O’Mill et al. (2011) and Brown et al. (2014), which modelled the K -correction needed for a given band as a simple (polynomial) function of a galaxy’s redshift and a quantity that characterises the SED of the galaxy. However, in this work we use the rest-frame colour for some pair of bands as that parameter, rather than an observed colour. This rest-frame colour can be determined using templates in a spectral regime where the range of galaxy SEDs is very well constrained, such as the optical rest-frame ($g - r$) band.

If we make the assumption that at low redshift galaxy SEDs can be approximated into a single parameter family – equivalent to assumptions made in that previous work – we show that with a single rest-frame colour we can match objects with equivalent SEDs across redshift, and thereby derive the dependence of K -corrections on the chosen rest-frame colour and redshift. With this approach, so long as one has access to a rest-frame colour that has been K -corrected already, one can then determine rest-frame colours for any other bands of interest. We caution that this assumption has only been tested extensively at low redshift ($z \ll 1$) with a limited Δz range; the situation may become more complex at higher redshift, where the assumption that SEDs fall into a single parameter family (Connolly et al. 1995; Madgwick et al. 2003a,b) or that K -corrections can be approximated as low-degree polynomials may break down. We presented an overview of this approach in Fielder et al. (2021), where we employed it to determine rest-frame WISE photometry; we describe and test this method more extensively in this work.

This paper is organised as follows. In Section 2.1, we briefly described the data used in our calculations, which includes GALEX, SDSS, 2MASS, and WISE observations. Section 2.3 details our method for determining K -corrections. In Section 3 we compare our computed rest-frame colours from our K -corrections to literature values. Finally, we summarise and discuss our findings in Section 4.

All magnitudes and colours are presented in the AB system in this work. Absolute magnitudes are determined using a Hubble constant $H_0 = 100 \text{ km s}^{-1} \text{ Mpc}^{-1}$, so they are equivalent to $M_y - 5 \log h$ (where M_y is the y -band absolute magnitude and $h = H_0/100$) for other values of h . Photometry is presented adopting the notation used in Blanton & Roweis (2007) and Licquia et al. (2015), where an absolute magnitude corresponding to passband y as observed at redshift z is denoted as $^z M_y$.

2 METHODS

2.1 Observational Data

The data used in this study originates from the GALEX-SDSS-WISE-Legacy Catalogue 2 (GSWLC-2) of Salim et al. (2016, 2018), within the redshift range of $0.01 < z < 0.09$. This data spans across the filter range of the GALEX ultraviolet survey FUV/NUV bands (Martin & GALEX Team 2005), the SDSS optical $ugriz$ bands (DR10; Ahn et al. 2014), the 2MASS near-infrared $JHKs$ bands (Skrutskie et al. 2006), and the WISE mid-infrared $W1/W2/W3/W4$ bands (Wright et al. 2010). Specifically, the WISE data is from the “unWISE” reduction of Lang et al. (2016) which is more appropriate for galaxies than the official pipeline. We use photometric data from the medium-deep

GSWLC catalogue, where the depth pertains to the UV photometry from GALEX, which unlike other bands is generally of much less uniform depth – going from shallow to very deep. While using the medium-deep instead of the shallow catalogue decreases the number of galaxies at our disposal by roughly one half, the increased signal-to-noise in the UV imaging is a worthwhile trade-off.

For objects within the GSWLC-M2 catalogue we have both the observed photometry (and associated errors) in addition to rest-frame values from the UV to the near IR (excluding WISE). These rest-frame values were obtained via fits to SED models, as described in Salim et al. (2016), which we summarise in Section 2.2. For convenience we convert the observed flux (f_ν) in Jy to AB magnitudes using the relation $m_{AB} = -2.5 \log_{10}(f_\nu) + 8.90$. As a result all magnitudes presented in this work are in the AB system.

In order to keep our galaxy sample at a maximum we split our data into four different catalogues: (1) a catalogue consisting of the SDSS $ugriz$ optical bands, (2) a catalogue consisting of the GALEX FUV/NUV bands and the $ugriz$ optical bands which we call UV+optical, (3) a catalogue consisting of the 2MASS $J/H/Ks$ near-IR bands and the $ugriz$ optical bands which we call near-IR+optical, and (4) a catalogue consisting of the WISE $W1/W2/W3/W4$ mid-IR bands, the $J/H/Ks$ near-IR bands, and the $ugriz$ optical bands which we call IR+optical. This way we can ensure that results from runs of KCORRECT are not driven by a specific set of bands. For example, an IR prediction can be entirely driven by a fit in the UV+optical depending on the signal-to-noise of the measurement, particularly because extrapolation is common for IR SED models.

Before we take further steps in our analysis we exclude all objects that have photometric values of “NaN”, infinity, or 0, which all indicate missing photometry. When evaluating the fits for the K -corrections we use a limited redshift range $0.04 < z < 0.09$ in order to avoid selection effects at low redshift ($0.01 < z < 0.04$), but compute K -corrections for the full redshift range of our sample. For the fits in the FUV/NUV bands we also exclude objects that have large GALEX photometric errors. Specifically, in FUV we perform the K -correction fits restricting to galaxies with errors $\sigma_{m_{FUV}} < 0.12$, while in NUV we require errors $\sigma_{m_{NUV}} < 0.1$. We apply similar cuts for objects that have large WISE photometric errors. These correspond to $\sigma_{m_{W1}} < 0.013$, $\sigma_{m_{W2}} < 0.025$, $\sigma_{m_{W3}} < 0.15$, and $\sigma_{m_{W4}} < 0.25$. These cuts were determined by examining distributions of the errors and how they biased the K -correction results. Before analysing our results we do a final clean to remove any “NaN” or infinity from each catalogue for the rare cases that an object did not have a proper fit in KCORRECT or our own analysis. Within our final wavelength separated catalogues the optical catalogue contains 148,704 galaxies, the UV+optical catalogue contains 28,318 galaxies, the near-IR+optical catalogue contains 74,038 galaxies, and the IR+optical catalogue contains 40,361 galaxies. Each spans from redshift $0.01 < z < 0.09$. The catalogues containing our K -corrected results and comparison values are publicly available at the catalogue section of our catalogue GitHub page.¹

2.2 K -corrections from Previous Work

We will be comparing our results from our fit calculations (described in the following subsection Section 2.3) to K -corrections from two other sources as a means to validate our results.

- (i) We generated K -corrections with the KCORRECT v4.3 software

¹ <https://github.com/cfielder/K-corrections/tree/main/Catalogs>

package [Blanton & Roweis \(2007\)](#). KCORRECT is a robust method for determining K -corrections using a combination of SED templates with SPS models, dust models, and nebular emission models. KCORRECT uses a non-negative matrix factorisation algorithm that creates model based template sets. A set of five template SEDs are used, which are derived from combinations of 450 [Bruzual & Charlot \(2003\)](#) SPS models across a wide range of age and metallicity, and 35 ionised gas emission models from [Kewley et al. \(2001\)](#). After the templates are generated and reduced into 5 sets, linear combinations of these templates are fit to the measured photometry and respective photometric errors for each galaxy for which K -corrections are being calculated with a χ^2 minimisation technique. This constructs an estimated SED for that galaxy. From the estimated SED K -corrections and other physical parameters can be determined.

We ran KCORRECT on the observed photometry and associated errors within the GSWLC-M2 catalogue for bands from the UV to IR composed of combinations of subsets of the wavelength range as described in [Section 2.1](#) in addition to the full wavelength range. KCORRECT can compute K -corrections for all filters considered in this paper (*FUV* through *W4*). We added an additional error term in quadrature to our inverse variance maggies equivalent to 1% of the respective observed maggy for the given band to allow for more flexibility in the models.

(ii) GSWLC ([Salim et al. 2016, 2018](#)) produces K -corrections by performing SED fitting using model SEDs. For this catalogue a Bayesian approach to SED fitting was employed ([Salim et al. 2007](#), see also [Kauffmann et al. 2003](#); [Brinchmann et al. 2004](#); [Tremonti et al. 2004](#) for the basis of this method) utilising the CIGALE SED fitting code ([Boquien et al. 2019](#)), which used a combination of ([Bruzual & Charlot 2003](#)) SPS models, dust models, and nebular emission models. In this approach millions of distinct models are considered individually, rather than utilising a linear combination of a smaller number of models (templates) like that performed by KCORRECT. Additionally, the GSWLC fits employ more recently updated models. In contrast to the best-fit (χ^2 minimisation) approach of SED fitting, such as that employed by KCORRECT, the Bayesian approach determines the full probability distribution of any parameter. This has the advantage of more robust parameter characterisation and uncertainty. The absolute magnitudes derived in the GSWLC catalogues are determined from the best fit model by comparison between the redshift model fluxes and the observations.

We simply adopt these rest-frame magnitudes directly from the catalogue, as the GSWLC-M2 catalogue serves as the basis for the data used in the analysis presented here so no additional conversions or calculations are necessary.

Results from KCORRECT and GSWLC-M2 provide two standards of comparison for our own derived K -corrections. One of the innate difficulties in determining K -corrections is the lack of a "true" answer for any observed galaxy. This makes it challenging to probe any differences between our own data driven approach and K -corrections from other template based approaches. Our goal is a method for which results are comparable to those from other approaches in regimes where we trust the SED templates and a technique that is easier to implement than those used by KCORRECT and GSWLC.

2.3 Deriving Data-Driven K -corrections

Our approach to determining K -corrections is based on the simplifying assumption that galaxy SEDs at low redshift can be approximated as a single-parameter family. This assumption stems from the results of applications of dimensionality reduction methods such as princi-

pal component analysis, which have found that the range of galaxy spectra at low redshift can largely be described with only a single parameter ([Connolly et al. 1995](#); [Madgwick et al. 2003a,b](#)). Likewise, previous work has shown that K -corrections can be approximated by an analytical function of redshift parameterised by a single quantity that characterises the intrinsic galaxy SED such as an observed colour ([Chilingarian et al. 2010](#); [O’Mill et al. 2011](#); [Beare et al. 2014](#)) or D_n4000 ([Westra et al. 2010](#)).

In this work, we leverage rest-frame colour information as the single parameter of choice; i.e., it serves as our means of distinguishing objects with intrinsically different SEDs. By choosing a rest-frame colour that can be well-determined by other K -correction methods, we can then bootstrap off of that reference colour to determine K -corrections for the rest of the SED. While the assumption of this direct mapping of a single rest-frame colour to SED shape is not perfect due to the ambiguity of contributions to the SED at fixed rest-frame colour (e.g., [Conroy 2013](#); [Magris C. et al. 2015](#)), it is sufficient to first order out to $z = 1$ ([Madgwick et al. 2003b](#)); in our primary applications, we consider galaxy samples that only span from $0.01 < z < 0.09$, so this is a reliable assumption.

Our approach for calculating K -corrections is to construct a function that produces rest-frame absolute magnitude given (1) the apparent magnitude of the band that needs to be corrected; (2) the apparent magnitude in a second band that serves as an “anchor”; (3) rest-frame colour in some pair of bands (which may include the anchor band but not the band which needs correcting; this rest-frame colour may be determined via any K -correction method of choice); and (4) redshift. K -corrections for the anchor band are also needed if we wish to determine rest-frame absolute magnitudes for the band that we wish to correct, but are not necessary if we only wish to determine rest-frame colours or SED shapes. We opt to use high signal-to-noise bands for the reference rest-frame colour and the anchor band; hence, we generally employ $(g - r)$ and m_r in this work. Some caution is warranted in this choice, however, as galaxies that span a large range in $(NUV - r)$ (4–6; i.e., green valley and truly quiescent galaxies) can end up with similar $^0(g - r)$ values around ~ 0.75 . However, for the UV bands we have tested other choices for rest-frame colours such as $^0(u - r)$ and found comparable K -corrected results to when $^0(g - r)$ is employed.

We approximate our K -corrections as a polynomial function of redshift with coefficients that are dependent upon rest-frame colour, multiplied by the observed (anchor - target band) colour. Thus, we utilise K -corrections that are defined by:

$$K_{\text{corr}} = f(z, ^0(A - B)), \quad (2)$$

where z is redshift and $^0(A - B)$ is a known rest-frame colour, $f(z, ^0(A - B))$ is a polynomial function of redshift to be determined.

To determine the parameters of the function $f(z, ^0(A - B))$ used to derive rest-frame colours, we perform a series of polynomial fits that are outlined in the following algorithm. These fits are tempered by various error cuts that determine which quantities are used for which fits, as described below. In the following, Y will refer to our generalised target band, which can be any band of interest except r , which we assume to be the anchor band.

(i) *The initial fits: Determining the dependence of the observed (anchor - target band) colour on redshift, in bins of rest-frame colour.*

We first wish to determine the polynomial relationships between the *observed* colour in a pair of bands (one of which serves as the anchor, and one of which is the desired target band) and redshift, for bins of fixed *rest-frame* colour in another (e.g., optical) pair of bands.

The relationship between these three quantities is exemplified in Fig. 1, where we plot observed $(r-i)$ colour as a function of redshift, with the points coloured according to each galaxy's rest-frame $(g-r)$. It is clear that the change in $(r-i)_{\text{obs}}$ with z depends upon both rest-frame colour and redshift. We analyse this dependence using small bins of rest-frame colour (~ 20 in total) with an approximately equal number of objects per bin. In the work presented here we use bins of rest-frame $(g-r)$ colour, but any other reliable colour measurement can be used.

In each bin we perform a polynomial fit to determine the relationship between observed colour and redshift at fixed rest-frame colour. We compute both linear and quadratic fits for all bands for comparison purposes but note that our work favours the linear approach in the cases we have explored to date, as discussed in Section 3.2. Our plots and tables generally provide results from linear fits for the initial polynomials only. The function we fit in each bin is defined as

$$(r-Y)_{\text{obs}} = f(z) = a_0 + a_1 z + a_2 z^2, \quad (3)$$

where a_0 is the constant term, a_1 is the linear coefficient, and a_2 is the quadratic coefficient. We fit for the parameters of Equation 3 using a Huber regression technique (Huber 1964), which is robust to outliers. These fits are implemented via `scikit-learn` (`sklearn.linear_model.HuberRegressor`; Pedregosa et al. 2011), where we set the parameter that controls the number of samples to be counted as outliers $\epsilon = 1.01$. A smaller ϵ will provide results that are more robust to outliers (one is the minimum value). For the linear case a_2 is set to 0. Thus, for each bin in rest-frame colour we determine the fit coefficients a_0 , a_1 , and a_2 simultaneously (or just a_0 and a_1 for the linear case).

Although we leave a_0 free when fitting, in the remainder of our procedures we fix its value at zero. This is necessary because when $f(z)$ is evaluated at a redshift of zero, its value would correspond to a_0 . As we have defined it, $f(z)$ corresponds to the offset between observed colour and rest-frame colour. However, **at redshift zero the K -corrections for all bands themselves must be zero**, as the observed and rest-frame bandpasses are identical in that case. Expressed in terms of Equation 3, it follows that $f(0) \equiv a_0 \equiv 0$.

In order to prevent higher-redshift objects from dominating the fits for observed colour vs. z in the redder $^0(g-r)$ bins due to their greater numbers, we employ a redshift-dependent weighting. To determine these weights, we split the objects within a single bin in $^0(g-r)$ into 40 bins in redshift space. Using these redshift bins and the counts in each bin N_{bin} we build an interpolating function $N_{\text{bin}} = g(z_{\text{cen}})$, where z_{cen} is the centre of the redshift bin, using the Virtanen et al. (2020) `scipy.interpolate.interp1d` algorithm. With this function we can pass in the redshift of each individual galaxy to obtain the value of N_{bin} at its z . The weights we use are then defined as:

$$w = \frac{1}{(NMAD(r-Y)_{\text{obs}})^2} \frac{<N_{\text{bin}}>}{N_{\text{bin}}}, \quad (4)$$

where $(NMAD(r-Y)_{\text{obs}})$ is the normalised median absolute deviation (NMAD) of the observed colour and $<N_{\text{bin}}>$ is the mean number of galaxies across the 40 bins. This down-weights bins with large numbers of objects, which has the greatest impact in the redder $^0(g-r)$ bins that are dominated by higher-redshift objects that otherwise skew the initial fits. These weights are then utilised in the aforementioned Huber regression of Equation 3 by assigning them as `sample_weight = w`.

As an example of the initial fit results we show the linear fits for observed $(r-i)$ as a function of redshift in Fig. 2. We have

elected to present 3 bins in $^0(g-r)$ instead of the full set of 22 for clarity. Each bin contains ~ 5435 galaxies. The points show all of the galaxies within the respective bin, while the black dashed lines show the result of the linear fit using Equation 3 ($a_2 = 0$). While the bin with blue points could also be fit by a quadratic, overall K -correction results proved to be more stable when we restrict all fits to be linear; this may not prove true in future applications.

(ii) *The secondary fits: Determining dependence of the initial fit coefficients upon rest-frame colour.*

Having obtained initial fits for each bin in rest-frame colour, we next fit for the linear dependence of each of the necessary fit coefficients (a_1 and possibly a_2) on the *mean* rest-frame colour within a bin. Since the value of a_0 must be zero (as described above), we make small adjustments to the observed photometry based only upon a_1 (and, if necessary, a_2) to obtain $^0(r-Y) = (r-Y)_{\text{obs}} + f(z)$.

We hence only need to determine a_1 and (if relevant) a_2 as functions of rest-frame colour. We express these fits as

$$a_1 = b_1 \langle ^0(g-r) \rangle + b_0 \quad (5)$$

and

$$a_2 = c_1 \langle ^0(g-r) \rangle + c_0, \quad (6)$$

where b_0 , b_1 , c_0 , and c_1 are fit coefficients and intercepts. Therefore we assume a linear dependence between each coefficient and the rest-frame reference colour. These fits are calculated using a Huber regression as before. For these secondary fits we also tested polynomials up to fifth order as well as logarithmic and exponential functions, but found that a linear fit performed just as well if not better than these more complex functions.

We exclude those colour bins for which the a_1 and/or a_2 values are highly uncertain from the fits to prevent them from influencing our results, as we found that in some bands the Huber regression produced unstable results when such bins were included. For each $^0(g-r)$ bin we calculate the NMAD of the residuals from the initial fit (i.e., the NMAD of the differences between the predicted $(r-Y)_{\text{obs}}$ value for each galaxy and its actual $(r-Y_{\text{obs}})$). Bins where the NMAD was more than $2.5\times$ larger than the minimum NMAD across all bins are excluded from the fitting of a_1 and a_2 as a function of mean rest-frame colour.

Fig. 3 illustrates the secondary fit for the i band. We plot the a_1 values determined from the initial fits (from step (i)) as a function of the mean $^0(g-r)$ for each bin as blue points. The black dashed line shows the linear function resulting from Huber regression for this "secondary" fit (Equation 5). For this band, none of the a_1 values were excluded by the NMAD cutoff.

Once this fit has been completed, the K -correction for individual galaxies can be determined by calculating a_1 and a_2 based on each one's rest-frame colours and then evaluating the resulting function $f(z) = a_1 z + a_2 z^2$ using that object's redshift.

(iii) *Determine whether to use a constant a_1 value instead of a linear fit.*

As mentioned above, although we tested using but linear and quadratic initial fits, the final derived K -corrections in this paper (as used in Fig. 9) will *all* be determined from purely linear fits (corresponding to $a_2 = 0$ in Equation 3). However, even with that simplification, for some bands we obtain more stable results by using a constant value of the a_1 parameter instead of having a_1 depend linearly upon rest-frame colour as in Equation 5. In these cases the a_1 's resulting from the initial fit varied little from each other, caus-

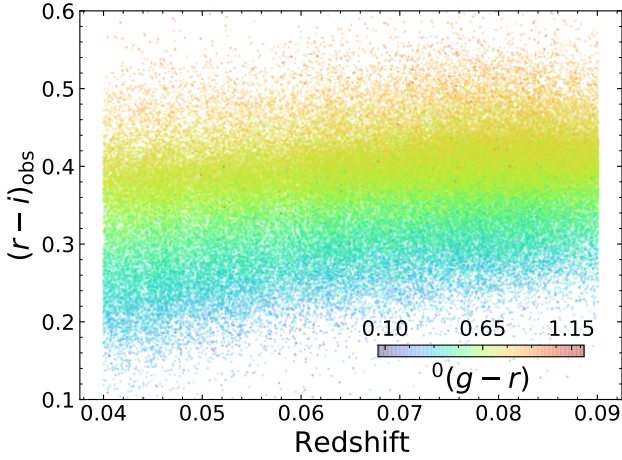


Figure 1. Observed $(r-i)$ colour plotted as a function of redshift for our galaxy sample. We have colour coded the points by rest-frame ${}^0(g-r)$ colour, where purple corresponds to more blue galaxies and red corresponds to more red galaxies. It is clear that observed colour is correlated with rest-frame colour and redshift. By determining fit coefficients in bins of rest-frame colour (cf. Fig. 2) we can quantify how the observed colour from a given pair of bands changes relative to the rest-frame colour across redshift space.

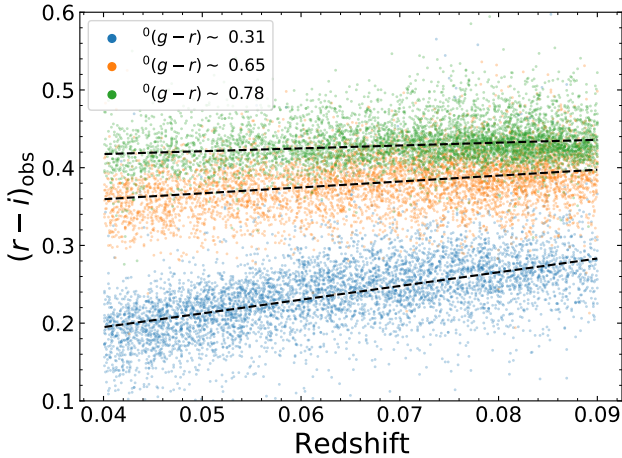


Figure 2. An example of our first-order polynomial fits to the redshift dependence of observed colour at fixed rest-frame colour. In this example we desire to K -correct i -band photometry, while the r -band serves as our anchor. We plot the observed $(r-i)$ colour as a function of redshift for three out of 22 equal-number ${}^0(g-r)$ bins constructed from the full sample; each bin includes ~ 5435 objects. The bins whose data is plotted are labelled according to the average ${}^0(g-r)$ colour within each. The black dashed lines represent the fits to Equation 3 for each bin plotted, performed using a robust Huber regression. The fits provide a reasonable representation of the trends within the data and are resistant to being pulled by outliers.

ing the secondary fit to be approximately a flat line. For such bands, instead of calculating a_1 as a function of mean rest-frame colour as described in step (ii), we simply use the median of the set of a_1 values across all rest-frame colour bins.

To determine whether to use a constant a_1 or the results of the secondary fit we take an information criterion-based approach. First we determine the NMAD of the a_1 values resulting from the initial fits (obtained from Equation 3). We label this normalised median

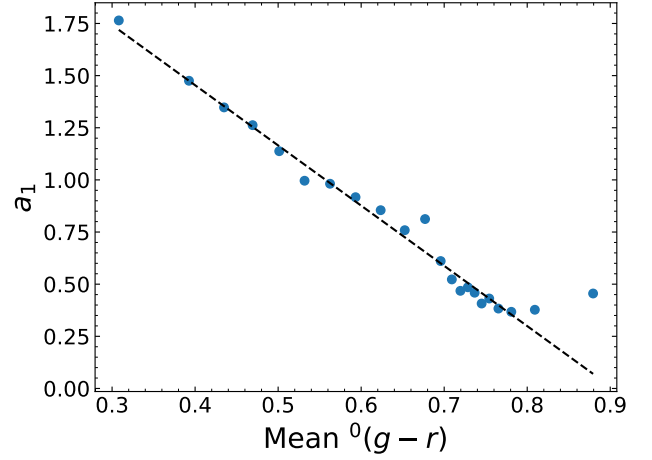


Figure 3. Linear-term coefficients (a_1) from the initial fit (i.e., the fit of observed colour as a function of redshift in bins of rest-frame colour, ${}^0(g-r)$, examples of which are shown in Fig. 2) are plotted as a function of the central ${}^0(g-r)$ of each bin using blue points. We perform a linear fit for a_1 as a function of the centre of a ${}^0(g-r)$ bins using a Huber regression (Equation 5), the result of which is plotted here as a black dashed line. A linear fit provides a good approximation to the plotted points. None of the a_1 values in this band were excluded from the fit by the NMAD cutoff, but the Huber regression is robust to the reddest and most discrepant point.

absolute deviation as σ_c ; so $\sigma_c \equiv \text{NMAD}(a_1)$. Then we determine the NMAD of the set of residuals $a_1 - a_{1,\text{pred}}$, which we label as σ . $a_{1,\text{pred}}$ are the a_1 values predicted by the secondary fit for a_1 as a function of ${}^0(g-r)$ (obtained from Equation 5) for each ${}^0(g-r)$ bin. If the residuals are entirely due to Gaussian random errors, this statistic should approximate the standard deviation of the error distribution.

The $\Delta\chi^2$ between the residuals for a constant a_0 versus those obtained when using the linear fit can then be approximated by

$$\Delta\chi^2 = N(1 - \frac{\sigma_c^2}{\sigma^2}), \quad (7)$$

where N is the total number of ${}^0(g-r)$ bins used in the initial fit in step (i) that pass the NMAD cutoff in step (ii). Then we define the quantity ΔAIC (which is based upon the Akaike Information Criterion, a quantity that can be used to test whether additional parameters meaningfully improve fits; Akaike (1974)) as

$$\Delta\text{AIC} = 2 + \Delta\chi^2, \quad (8)$$

as the linear fit has a total of two free parameters. For photometric bands where $\Delta\text{AIC} < -10$ we use a linear fit for a_1 ; however, when $\Delta\text{AIC} \geq -10$, indicating that there is at most moderate evidence that a linear fit performs better, we instead set the a_1 value to a constant corresponding to the median of the a_1 's determined in step (i).

In this work, a constant a_1 value was favoured for the J , H , Ks , $W1$, $W2$, $W3$, and $W4$ bands when fits were performed for a_1 as a function of $K\text{CORRECT } {}^0(g-r)$ colour. When instead $\text{GSWLC-M2 } {}^0(g-r)$ colour was used, a constant a_1 was favoured for z , Ks , $W1$, $W2$, and $W4$. All other bands use what we refer to as a “linear” a_1 dependence on rest-frame colour, corresponding to Equation 5.

(iv) *Determine rest-frame colours and/or absolute magnitudes using the coefficient fits.*

At this stage we now have a function that predicts the difference between the observed colour $(r-Y)$ and rest-frame ${}^0(r-Y)$ as a

function of both an object's rest-frame colour in another pair of bands and the redshift. Since the value of a_0 must be zero (as described in step (i) above), we can re-write Equation 3 as:

$$(r - Y)_{\text{obs}} = {}^0(r - Y) + a_1 z + a_2 z^2. \quad (9)$$

Thus by subtracting $a_1 z$ and $a_2 z^2$ from the observed colour, the rest-frame colour in that pair of bands can be obtained; i.e., we have calculated a K -corrected colour. We can solve for the rest-frame colour, obtaining:

$${}^0(r - Y) = (r - Y)_{\text{obs}} - a_1 z - a_2 z^2 = m_r - m_Y - a_1 z - a_2 z^2. \quad (10)$$

If one is interested in determining the absolute magnitude in rest-frame band Y instead of the rest-frame $r - Y$ colour, then one **must** have access to a K -corrected version of the anchor band. To solve for 0M_Y instead of ${}^0(r - Y)$, we exploit the fact that ${}^0(r - Y) = {}^0M_r - {}^0M_Y$, which we can rearrange to obtain:

$${}^0M_Y = {}^0M_r + {}^0(r - Y), \quad (11)$$

where ${}^0(r - Y)$ can be determined from Equation 10. 0M_Y should then correspond to the K -corrected absolute magnitude in band Y .

(v) Determine errors on K -corrections²

Having determined the values of the K -corrections of interest, we next wish to estimate their uncertainties. Since the results presented in this paper are all derived from either a linear fit for the a_1 's or by using a constant a_1 value, we describe our procedures for the case of linear fits; the methods we use can also be applied in other scenarios, however.

Specifically, we estimate the errors in K -corrected photometry by applying propagation of errors to Equation 10. The resulting formula is:

$$\sigma({}^0(r - Y)) = \sqrt{\sigma_{m_r}^2 + \sigma_{m_Y}^2 + (z\sigma_{a_1})^2}. \quad (12)$$

We have dropped the $a_2^2 \sigma_z^2$ term here, as σ_z is negligible for galaxies with spectroscopic redshift measurements.

Thus, to calculate the uncertainty in ${}^0(r - Y)$ we will need to determine σ_{a_1} . For bands where a_1 is treated as linear in rest-frame colour, we determine σ_{a_1} via bootstrap re-sampling (Efron 1979). We construct 100 sets of matched mean ${}^0(g - r)$ and a_1 values, each of equal size to the original data set used in the fit, but with each original (mean ${}^0(g - r)$, a_1) pair having equal probability of being chosen for each element of the new set of pairs that will be fit to (i.e., we perform bootstrapping of the original set of values from the fits in rest-frame colour bins, with replacement). For each of these hundred bootstrapped data sets we perform a Huber regression as in step (ii), fitting for Equation 5, which yields 100 sets of b_0 and b_1 values. Then for each galaxy we can determine 100 a_1 's via Equation 5 by plugging in the galaxy's ${}^0(g - r)$. Finally, we calculate the standard deviation of the bootstrapped a_1 values for each object, providing an estimate of the appropriate σ_{a_1} value for it.

When a_1 is treated as a constant, bootstrapping is not necessary to determine its uncertainty. Instead we estimate its value as $\sigma_{a_1} = \frac{\text{NMAD}(a_1)}{\sqrt{0.64N}}$, where N is the number of colour bins used, as the standard deviation of the median of N values drawn from a Gaussian distribution of standard deviation σ is approximately $\frac{\sigma}{\sqrt{0.64N}}$ (Maidonald & Braun 2010).

For convenience purposes, we generally quote photometric errors (e.g., σ_{m_Y}) separately from the uncertainty in the K -correction ($z\sigma_{a_1}$). When a single net uncertainty is needed (e.g., for plots), we combine errors in quadrature, following Equation 12.

Tables of the b_0 and b_1 values needed to determine a_1 for arbitrary ${}^0(g - r)$ values, as well as the median a_1 values across all bins, are provided in Table A1 (KCORRECT derived) and Table A2 (GSWLC-M2 derived) of Section A. The Python functions used to determine our b_0 , b_1 , and median a_1 values and related quantities in addition to sample code are provided at our *K-correction* GitHub² page for public use. These materials allow K -corrections for low-redshift objects to be calculated easily for any of the bands considered in this paper.

3 RESULTS

We test our results by comparing to two other K -correction methods performed on the same data: the standard software KCORRECT, and SED fitting results from the GSWLC-M2 catalogue (Salim et al. 2016, 2018) which are described in Section 2.1. In our work the rest-frame values from which we determine our fits are from either the GSWLC-M2 catalogue calculations or the KCORRECT calculations. Depending on which K -correction method we wish to compare our calculations to we use the respective rest-frame colour.

While there are discrepancies between K -corrections calculated between any two methods, with our results in general agreement with other methods for well-behaved bands we can be confident in our simplified approach.

3.1 Distributions of Rest-frame Colours

We start with a generalised comparison to KCORRECT and GSWLC-M2. In Fig. 4 normalised histograms depict results for colours across the wavelength range. We derive these respective to the catalogue to which they are being compared. For example we derive ${}^0(u - r)$ utilising ${}^0(g - r)$ from KCORRECT when comparing to KCORRECT results. The step histograms denote our derived results, and the lightly shaded histograms denote results from the two comparison methods. Blue histograms come from KCORRECT and orange histograms come from GSWLC.

Foremost, we do not expect all results to be 1 : 1 with each other due to the nature of fitting and how the K -corrections are approximated in each method. The relatively large scatter of individual K -corrections has been exemplified in the literature (see e.g., O'Mill et al. 2011, Fig. 3, Chilingarian et al. 2010, Fig. 2). We do find that, in general, the distributions of our K -corrected colours are in good agreement with those derived from other methods. In many cases our results are in better agreement with the respective comparison work than KCORRECT and GSWLC-M2 are with each other. However, there are some notable differences.

Our results in the 2MASS bands from either derived source are in excellent agreement with each other and the results from KCORRECT. However, the GSWLC-M2 results are more peaked. Such discrepancies in the near-IR 2MASS bands in the GSWLC-M2 catalogue may result from a couple of factors. Templates in the IR are typically of lower quality than in the optical, particularly because there are few spectra fully observed from the UV-IR. Therefore some assumptions are required in the less constrained bands. For example, there is uncertainty of how asymptotic giant branch (AGB) stars contribute to stellar population synthesis models. In particular, thermally pulsating AGB (TP-AGB) stars may contribute a significant portion of light to the IR portion of an SED but how much is unknown (Conroy 2013).

² <https://github.com/cfielder/K-corrections>

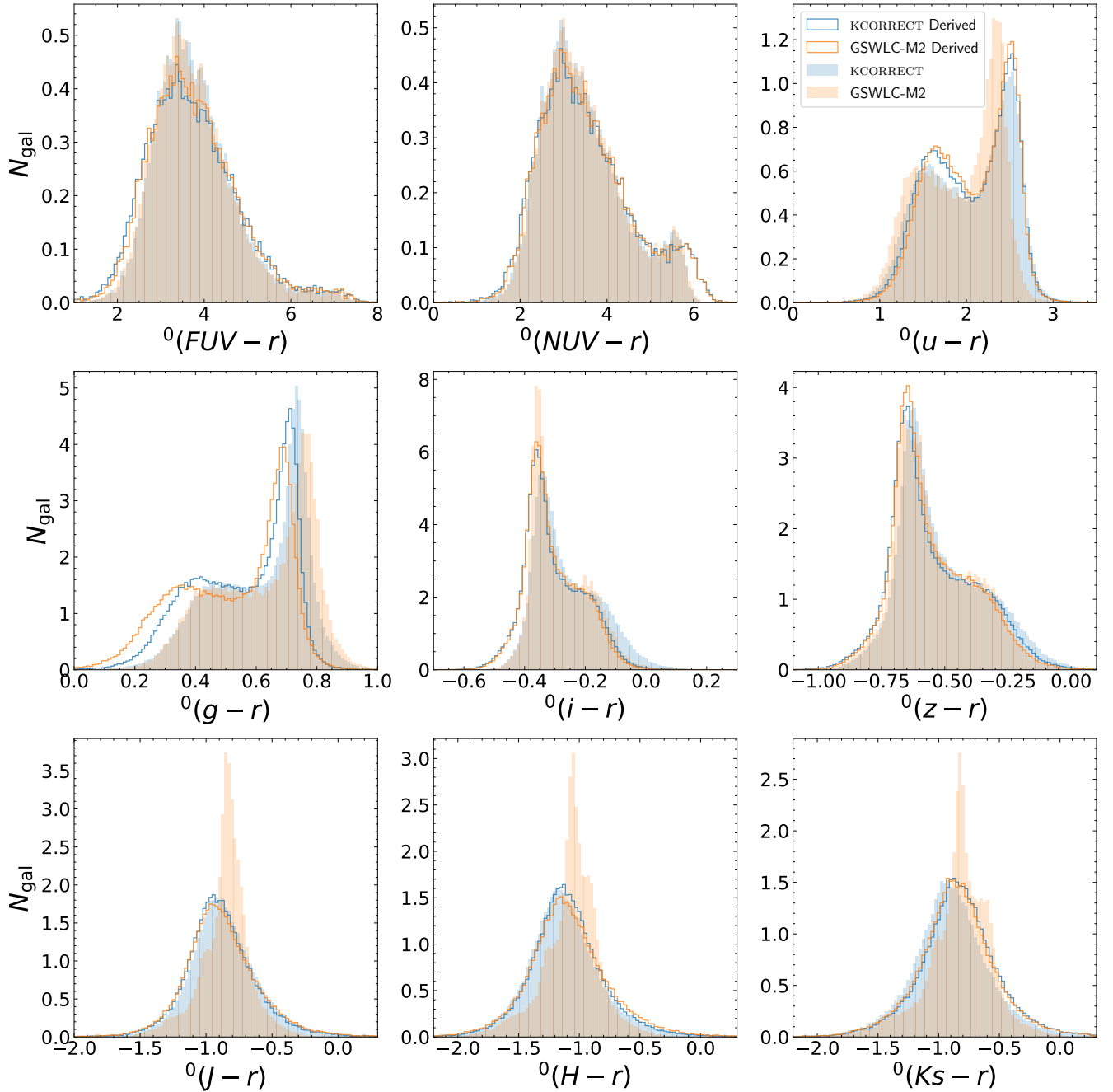


Figure 4. Histograms of rest-frame colours comparing K -correction methods for GALEX FUV/NUV , SDSS $ugiz$, and 2MASS $J/H/Ks$ bands. We show our calculated rest-frame colours derived from KCORRECT (blue line) and GSWLC-M2 (orange line) and those calculated using the KCORRECT software (blue shaded) or in the GSWLC-M2 catalogue (orange shaded). In general, our rest-frame colours derived from both KCORRECT and GSWLC-M2 are in excellent agreement with each other. In the 2MASS bands, our rest-frame colours derived from KCORRECT and GSWLC-M2 are self-consistent and in agreement with the KCORRECT colours; however, the GSWLC-M2 colours show more peaked distributions likely caused by uncertainties in modelling unusual older stellar populations (TP-AGB stars, post-AGB stars, and extreme HB stars). The offsets in $^0(g-r)$ are likely due to the fact that our rest-frame colours are derived from $^0(g-r)$ for both catalogues. Overall, our rest-frame colours for these bands are well-matched to each other and to those from KCORRECT and GSWLC-M2.

The IR portion of the SED is also further complicated by contributions of dust emission. It is likely the case here that the discrepancy of the GSWLC-M2 results is driven by the SED fits preferentially constrained in the UV and optical where models have more certainty.

While small, we note that discrepancies in the FUV , NUV , and u bands are likely a result of (1) the high sensitivity of UV colours to minimal amounts of star formation, (2) the uncertainty of con-

tributions of post-AGB and extreme horizontal branch stars, and (3) complexity of dust absorption and scattering (see e.g., [Conroy 2013](#)). Simple stellar populations, which are the backbone of SPS model SED based approaches, may not adequately capture the UV sensitivity to star formation, and dust and unusual stellar populations further complicate these effects.

In [Fig. 4](#) it appears that there are also discrepancies of note in

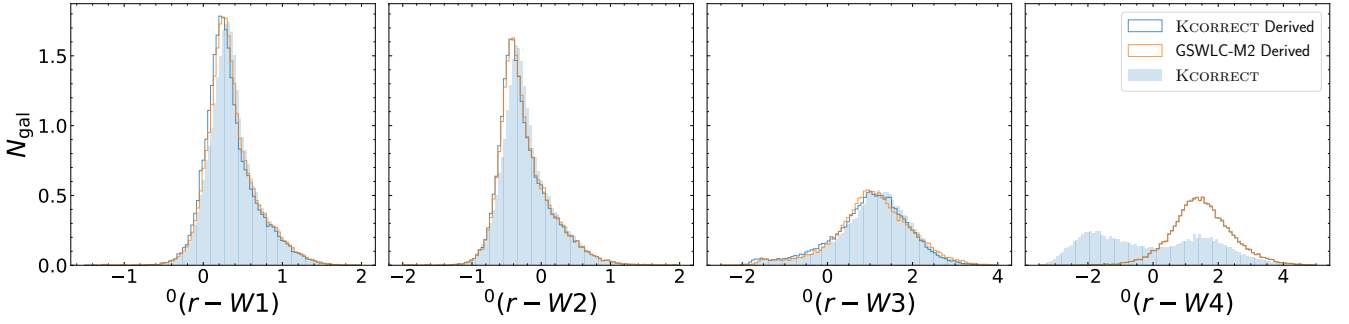


Figure 5. Same as Fig. 4 but for the WISE bands. GSWLC-M2 did not derive WISE colours, but we still derive rest-frame WISE colours using $^0(g-r)$ from both KCORRECT and GSWLC-M2. Our results derived from either source agree well with each other. Additionally, histograms match well with those of KCORRECT, except for the W4 band, which we suspect is a result of a template error in KCORRECT. This discrepancy in W4 highlights an advantage of deriving K -corrections independent of templates in poorly constrained bands.

the optical bands (particularly g and i). However, across wavelength space the differences between results are no more than ~ 0.1 magnitudes and agree on average at the 0.05 magnitude level after exploration of the NMAD and root mean squared error between our results and the respective literature result. Differences are more pronounced in the optical given the narrow range of colour space that they span. While the $^0(g-r)$ results presented here are calculated in bins of $^0(g-r)$, which is redundant, we also derived $^0(g-r)$ from computing $^0(g-i)$ and $^0(r-i)$ in bins of $^0(g-r)$ and then combining results. The results were similar, so we present the more straightforward result here. We want to emphasise that the bluest galaxies in KCORRECT and GSWLC-M2 have derived $^0(g-r)$ colours redder than ours starting at $z \sim 0.03$. Additionally, the rest-frame colour derived from the SED fitting techniques is *redder* than the observed colour for these very blue objects, contrary to the expected blue-ward shift in the optical post K -correction. The likely culprit is either a lack of SED templates for the most extremely blue galaxies, or some lacking or excess contribution from the dust absorption and nebular emission models. Investigations in small redshift bins of rest-frame $(g-r)$ colour show that the red sequence is more consistent at different redshift with our K -correction method than $^0(g-r)$ colour derived using KCORRECT.

Fig. 5 depicts the same comparisons as Fig. 4 for the WISE bands. The GSWLC-M2 did not perform SED fitting directly with the WISE bands (Salim et al. 2018), so those values are not included. Overall, we observe very consistent results with those of KCORRECT except in the W4 band. This miss-match in distributions between results of KCORRECT and the distributions of the observed photometry and our own derived rest-frame photometry can largely be attributed to the lack of dust emission modelling in KCORRECT. Therefore any rest-frame W2 through W4 results obtained via KCORRECT could be incorrect due to the lack of these types of models.

To check the performance of our K -corrections we examine colours in small redshift bins. We choose narrow bins as there should be minimal colour variance across the galaxy sample, meaning they should all have approximately the same observed frame SED. Fig. 6 shows results of this analysis for a selection of colours across our wavelength range. We plot contours for $0.04 < z < 0.045$ (blue) and $0.075 < z < 0.08$ (orange). On our x-axis we plot $^0(g-r)$. The left column depicts contours using observed colours and the right column depicts contours for rest-frame colours. These specific rest-frame colours are derived from KCORRECT $^0(g-r)$. For objects that have been properly K -corrected, the contours should line up better in the rest-frame column than the observed-frame column. This is

indeed the case for our bands, which indicates that our K -corrections are working as expected. Plots made for KCORRECT and GSWLC-M2 rest-frame colours can be made, with similar results, save for $(W4-r)$ which is dramatically offset in the KCORRECT results. While $(FUV-r)$ exhibits minimal change, this is also the case for KCORRECT and GSWLC-M2.

3.2 Extrapolations to $z=0$

At redshift 0, by definition a K -correction must be 0. This means that any difference between observed colours (or magnitudes) and rest-frame colours (or magnitudes) at redshift 0 must also be 0. As we showed in Section 2.3 our K -corrections are defined to follow this relationship. However, this is not enforceable for methods that incorporate SED/template fitting. We compare our K -correction colours to that of KCORRECT and GSWLC-M2 in Fig. 7 and Fig. 8 for optical and UV/near-IR bands, respectively. We plot the colour difference as a function of redshift where, for example, $\Delta(u-r) = (u-r)^0 - (u-r)$ or the difference between the observed-frame colour and rest-frame colour. We specifically plot the means of these colour differences across 12 bins in redshift space. Blue points correspond to K -corrected results using our method with a linear fit and orange points correspond to K -corrected results using our method with a quadratic fit. Grey points correspond to results from KCORRECT (left column) and GSWLC (right column).

The blue points also have representative error bars plotted that include both systematic errors and K -correction errors, for which the K -correction errors are described in (v) of Section 2.3. We must take a few additional steps for these plots, as we are showing the means in bins. The error attributed to the K -correction does *not* diminish when determining means. So for the K -correction error we simply compute $\langle \sigma_{a1} z \rangle$. We define the random error on the mean as $\sigma_{sys} = \frac{\sigma(\Delta)}{\sqrt{N_{bin}}}$. The total error on the means is thus these two contributions added in quadrature.

Because our galaxy sample only extends down to redshift 0.01, we must extrapolate to $z = 0$. This is done with a linear interpolation for colour difference as a function of the redshift of the bin centre (z_{cen}), utilising the `scipy.interpolate.interpld` class from Virtanen et al. (2020). These extrapolations are plotted as dashed lines, which ideally should pass through the origin. Our linear and quadratic fits do so in most cases (with some scatter), in contrast to fits from KCORRECT and GSWLC-M2 for many bands. This directly demonstrates the improved accuracy of our K -correction method compared to SED-

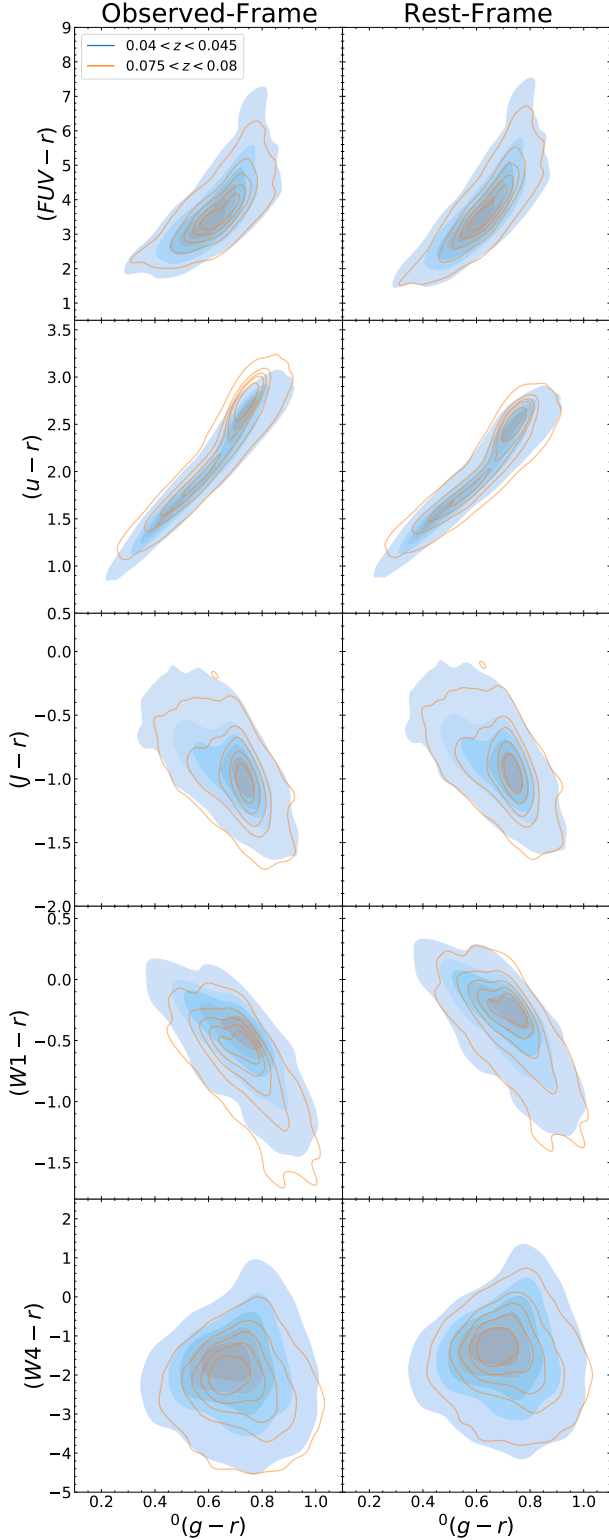


Figure 6. Contour plots of galaxies in two narrow redshift bins $0.04 < z < 0.045$ (blue) and $0.075 < z < 0.08$ (orange). We plot a variety of colours across our wavelength range as a function of $^0(g - r)$. The left column shows these colours in the observed-frame and the right shows these colours in the rest-frame, using our K -correction results. We plot narrow redshift bins as the observed SEDs of the galaxies should be approximately the same. It is evident that for all colours the contours of both redshift bins align closely in the rest-frame in contrast to the observed-frame. This is the expected result for successful K -corrections and similar results are observed in Kcorrect and GSWLC-M2 (save for $(W4 - r)$).

fitting K -correction methods. Additionally these figures exemplify that in most cases a linear function of redshift is a better choice than a quadratic one for deriving our relationship between observed colour, redshift, and rest-frame colour. First, the linear fit derives very comparable results to the quadratic fit and is much simpler to implement. Second, the linear fit results more consistently pass through the origin than the quadratic fit results. It is also worth noting that despite the difference in the techniques, the relative shapes of the results in both Kcorrect and GSWLC-M2 agree well. Likewise the relative shapes of our results, regardless for which source the rest-frame band is used, are also in agreement in both linear and quadratic initial fits.

3.3 Spectral Energy Distributions

Spectral energy distributions (SEDs) are an excellent test of our K -correction results. In this subsection we compare our K -corrected rest-frame photometry to that of our other sources of K -corrected photometry and the observed photometry for a couple of galaxies. Because our galaxy sample is at such a low redshift, the K -correction in each band should be relatively small and mirror the shape of the observed SED.

To determine luminosity we use similar derivations to those presented in Section 4.3 of Fielder et al. (2021), which we also summarise here. Because the r -band serves as the anchor in our K -correction derivations we can derive fluxes relative to the r -band. We use 0M_r from Kcorrect and GSWLC-M2 respective to which K -correction source we compare to. The luminosity of r -band is derived as

$$\log(\nu_r L_{\nu,r}) = \log \nu_r + \frac{(^0M_r - 34.04)}{-2.5}, \quad (13)$$

which is derived from the relation for converting flux to AB magnitudes in combination with the area of a 10 pc radius sphere to convert flux to luminosity. The error on this quantity via propagation of errors is equivalent to

$$\sigma_{\log(\nu_r L_{\nu,r})} = 0.4 \sigma_{^0M_r}. \quad (14)$$

For the other bands we use our derived colours $^0(r - Y)$ to first determine the flux ratio relative to the r -band

$$\log\left(\frac{f_{\nu,r}}{f_{\nu,Y}}\right) = \frac{^0(r - Y)}{-2.5}. \quad (15)$$

This formula is based on the definition of observed AB magnitude. We can then derive luminosity for other bands utilising the equivalence of flux ratios to luminosity ratios. Our final SED luminosities are

$$\log(\nu_Y L_{\nu,Y}) = \log(L_{\nu,r}) - \log\left(\frac{f_{\nu,r}}{f_{\nu,Y}}\right) + \log(\nu_Y), \quad (16)$$

where $\log(\nu_Y L_{\nu,Y})$ is in units of Watts. The corresponding errors are defined as

$$\sigma_{\log \nu L_{\nu,x}} = 0.4 \sqrt{\sigma_{^0M_r}^2 + \sigma_{^0m_Y}^2 + (z\sigma_{a_1})^2 \sigma_{^0M_r}^2}, \quad (17)$$

which can be derived from propagation of errors and plugging Equation 10 into Equation 15.

In Fig. 9, we plot the SEDs of two galaxies from our sample. These galaxies share the same $^0(g - r)$ colour of 0.667 but reside at two different redshifts with the lower redshift galaxy plotted in blue and the higher redshift galaxy plotted in orange. The normalisation of the lower redshift object is offset such that the two galaxies can be plotted without overlap. Open circles with error-bars show results

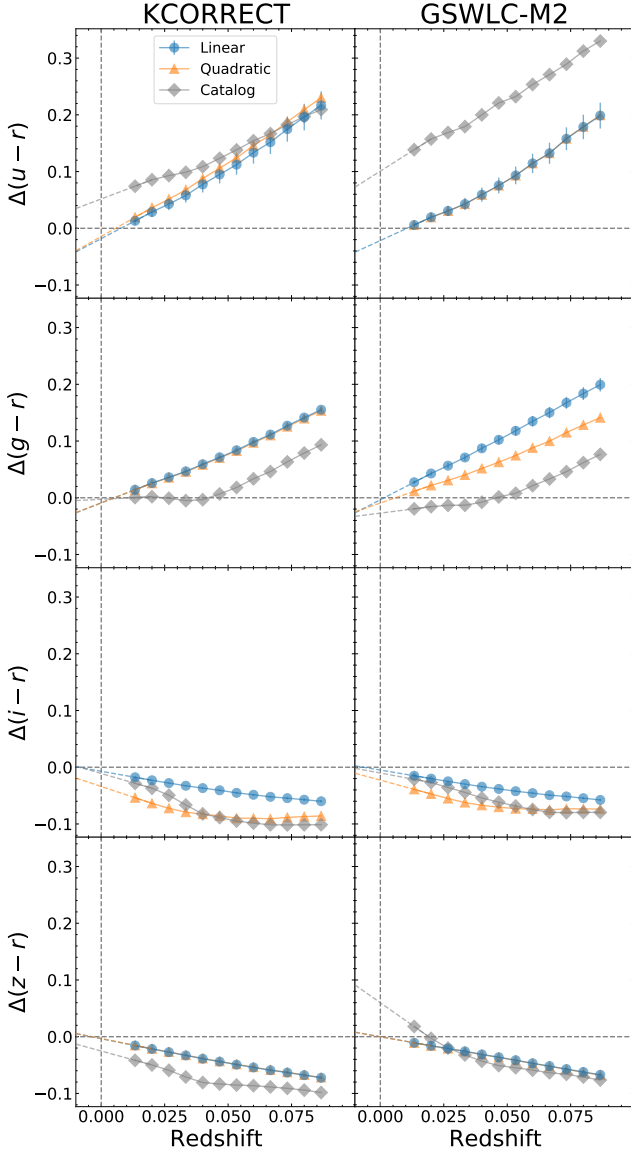


Figure 7. Plots of the mean difference between observed and rest-frame colour (e.g., $\Delta(u-r) = (u-r) - {}^0(u-r)$) as a function of 12 redshift bins for optical colours. Blue points depict our K -corrected results with a linear initial fit, and orange points depict results for a quadratic fit. Grey points show results from the corresponding source denoted at the column title. The coloured dashed lines depict a linear extrapolation to redshift 0. Our results all approach the origin closely, as they should by construction and under the expectation that at redshift 0 the K -correction should be 0. However, this is not necessarily the case for K -corrections that rely on SED fitting.

from our work, which are derived using either a linear or constant a_1 in Section 2.3. For all bands other than r , we do not plot the σ_{0M_r} term in Equation 17 as this error is covariant across all bands. This quantity is small and challenging to infer from the plots; $\sigma_{0M_r} = 0.0012$ for the low redshift plot and $\sigma_{0M_r} = 0.0032$ for the higher redshift plot. Triangular points show the K -corrections for these galaxies from KCORRECT (left panel) and GSWLC-M2 (right panel). Lastly, star points show the observed fluxes of the same galaxies, normalised to match in the r -band.

As a means to compare these two galaxies we also plot an SED template galaxy from the Brown et al. (2014) nearby galaxy SED

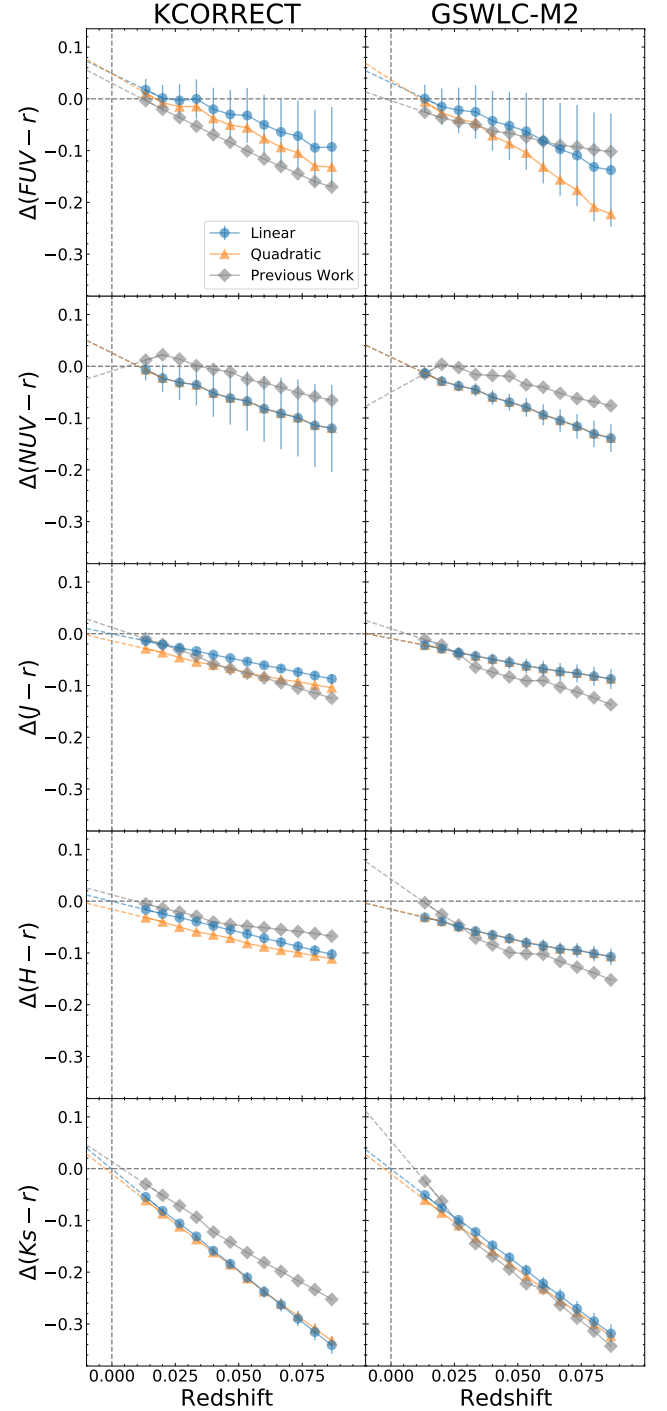


Figure 8. Same as Fig. 7 but for UV and near-IR bands. Our results perform just as well as if not better than those from SED fitting.

atlas - NGC 4138. The magnitudes of the templates were converted to fluxes (as described in 4.2.2 of Fielder et al. 2021 utilising the AB magnitude definition), and then normalised in r -band. For each of the 129 galaxy SED templates in the atlas we calculate the chi-squared of the difference between the brightness of each of our selected galaxies and that of the templates:

$$\chi^2 = \sum \left(\frac{\log \nu L_{\nu}^{\text{atlas}} - \log \nu L_{\nu}^{\text{galaxy}}}{\sigma_{\log \nu L_{\nu}}} \right)^2. \quad (18)$$

$\sigma_{\log \nu L_\nu}$ combines in quadrature the total error in the galaxy SED for a given band, the uncertainties in the [Brown et al. \(2014\)](#) photometry, and $\log_{10}(1.1)$, which corresponds to a 10% error in νL_ν . This additional 10% error is added to account for systematic uncertainties in the photometry such that optical bands do not dominate the χ^2 values given their intrinsically small uncertainties.

The template plotted in grey in [Fig. 9](#) corresponds to the spectrum of the NGC 4138 template, which had the smallest χ^2 compared to *both* galaxies selected from our sample. Dashed portions of the plotted template indicate regions of the spectrum that were modelled, while solid portions of the template indicate regions of the spectrum that were observed. We do not expect this template to directly match the photometry of either selected galaxy but to provide a means of comparison. This spectrum also exemplifies the use of modelling required in the UV and IR for empirical SED templates.

One can draw several conclusions from [Fig. 9](#). First, our K -corrected photometry is reasonably close to that of other methods of producing K -corrected photometry in addition to the observed photometry. At our low redshift range the rest-frame photometry should not be substantially different from the observed photometry, which is the case for our results. When combined, we have results that resemble an SED reasonably well, while making minimal assumptions about how an SED *should* look.

Second, it is evident that K -CORRECT fails in giving a reasonable result for W4 band K -corrections which is further supported by the results shown in [Fig. 5](#). In [Fig. 9](#) the brightness of the lower redshift galaxy's W4 band from K -CORRECT is so low that it overlaps with the other galaxy's observed brightness. For the higher redshift galaxy the W4 point is below the y-axis range. Our K -correction approach supplies reasonable results for W4. By construction our method cannot stray too far from the observed photometry, so even bands like W4 that have low signal-to-noise ratios can be reasonably constrained. In that same vein our K -correction method has more flexibility than standard SED fitting where multiple bands are forced to match the templates.

4 CONCLUSIONS

In this work, we present a new, empirically-driven method for obtaining K -corrections. Our method is inspired by the polynomial based K -correction methods of [Beare et al. \(2014\)](#) and [Chilingarian et al. \(2010\)](#), where we exploit the parameterisation of K -corrections by an analytical function of redshift and colour (see also [Willmer et al. 2006](#); [O'Mill et al. 2011](#)). At low redshift ($z < 1$), SEDs fall into a single parameter family where a single rest-frame colour allows us to infer the full SED shape - an inference made from results describing spectra by a single parameter in reduced dimensional space ([Connolly et al. 1995](#); [Madgwick et al. 2003a,b](#)). Our method limits the dependence on SED templates by interpolating using a rest-frame colour for which SEDs are well-constrained. We perform a series of linear fits to construct a function that maps observed colour and redshift to rest-frame colour.

There are a number of pieces of evidence that prove our data driven approach to determining K -corrections is yielding sensible results. Throughout this work we compare to the oft-used K -CORRECT v4.3 software of [Blanton & Roweis \(2007\)](#) and the derived results in the GSWLC-M2 catalogue ([Salim et al. 2016, 2018](#)), both of which utilise SED fitting in different ways (see [Section 2.2](#)). Our K -corrected photometry is in agreement with K -corrected photometry of the same objects for both comparison methods, particularly at UV and optical wavelengths (see e.g., [Fig. 4](#)). Likewise our

K -corrected photometry produces sensible looking galaxy SEDs, similar to both comparison methods (see [Fig. 9](#)). We also have better agreement across redshift in colour-colour space with our rest-frame colours than our observed-frame colours, as exemplified in [Fig. 6](#). This is the expected behaviour of photometry that has been correctly K -corrected. Lastly, our K -corrections go to zero at redshift zero, as shown in [Fig. 7](#) and [Fig. 8](#), as expected by the definition of the K -correction. However, SED fitting methods cannot directly enforce this, as exemplified by their differences in the figures. Our method is driven by and stays close to the observations in the band of interest rather than follow a model which can yield larger deviations. This allows us to K -correct bands that are poorly constrained by templates and have low signal-to-noise ratios.

There are also notable discrepancies between our K -corrected photometry and that of K -CORRECT and GSWLC-M2, which mostly occur in the infrared bands. First, as seen in [Fig. 4](#), the rest-frame photometry in the 2MASS $JHKs$ bands is more peaked compared to the other histograms. However, our derivations from both K -CORRECT and GSWLC-M2 are in excellent agreement with each other and that of K -CORRECT. This highlights one of advantage of our approach. SED model uncertainties in the IR due to contributions from AGB stars may result in incorrect K -corrections. Higher signal-to-noise optical portions may also drive SED fits resulting in incorrect K -corrections. Empirical SED models are also more poorly constrained at non-optical wavelengths due to a lack of spectral measurements that in turn produce uncertain SED fits. The other notable discrepancy is that of the WISE W4 band, noted in [Fig. 5](#) and [Fig. 9](#). The predicted K -CORRECT W4 band rest-frame photometry is severely offset from our predictions, while our results utilising either K -CORRECT or GSWLC-M2 optical colours are in good agreement with each other and with K -CORRECT results in the other WISE bands. We suspect that the K -CORRECT templates are making un-physical assumptions, yielding an unexpected result. Most notable is the lack of dust emission modelling in K -CORRECT, a feature of increasing importance for the WISE bands. In contrast, our data-driven approach entirely avoids issues of template fit failures and model issues by only relying on well-constrained rest-frame optical colours.

Our data driven K -correction approach is particularly suitable for calculations in bands where templates are not well constrained or readily available. In our previous work of [Fielder et al. \(2021\)](#) in constructing a UV-IR SED for the Milky Way we required WISE-band K -corrections - bands sensitive to dust content and dust luminosity (which are consequently a constraint on star formation rate, see e.g., [Salim et al. 2018](#)). Because WISE-band K -corrections were not readily accessible we developed the approach presented here for determining K -corrections.

ACKNOWLEDGEMENTS

Authors Catherine Fielder, Brett Andrews, and Jeff Newman gratefully acknowledge support from NASA Astrophysics Data Analysis Program grant number 80NSSC19K0588 which made this research possible.

This work made use of PYTHON, along with many community-developed or maintained software packages, including IPython ([Perez & Granger 2007](#)), Jupyter ([jupyter.org](#)), Matplotlib ([Hunter 2007](#)), NumPy ([van der Walt et al. 2011](#)), Pandas ([McKinney 2010](#)), scikit-learn ([Pedregosa et al. 2011](#)), and SciPy ([Virtanen et al. 2020](#)). This research made use of NASA's Astrophysics Data System for bibliographic information.

This paper was based in part on observations made with the

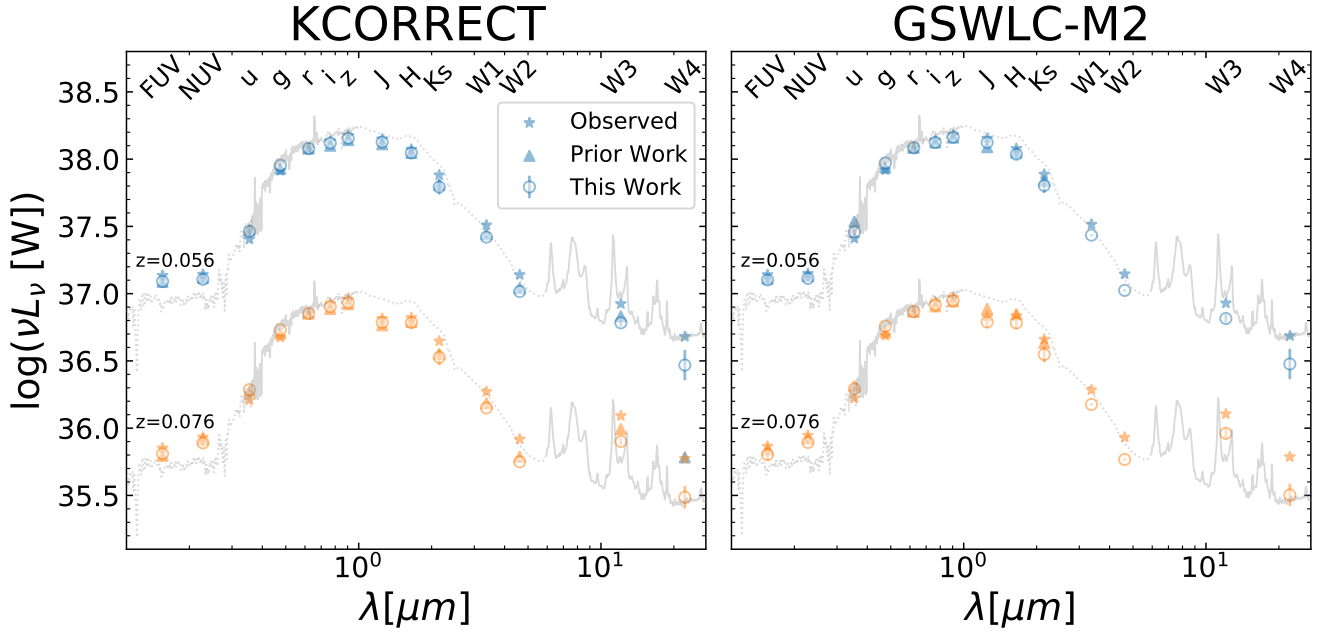


Figure 9. Derived SEDs for two galaxies from our sample which share the same $^0(g-r) = 0.667$ but reside at two different redshifts. The lower redshift galaxy is plotted with blue points and offset from the higher redshift galaxy in the y-axis for clarity. Stars are plotted at the observed fluxes. Triangles are plotted at the luminosity determined from the rest-frame magnitudes derived via KCORRECT (left panel) and GSWLC-M2 (right panel). Circles with error bars show our resulting luminosities from our K -correction method. As a means of comparison we plot the spectrum of NGC 4138 from the Brown et al. (2014) galaxy SED atlas in grey, with dashed lines showing modelled portions of the spectra and solid lines showing the observed portions of the spectra. This template had the lowest χ^2 of the difference between the photometry of the two galaxies shown and the template (normalised in r -band). While we do not expect a direct match to a template, we provide it as a means of comparison to help guide the eye. We can conclude that our K -correction method provides reasonable estimates for even the weakly constrained WISE bands, where KCORRECT fails in W4 and GSWLC lacks. The rest-frame W4 prediction of the higher redshift galaxy lies below the y-axis range and the rest-frame prediction for the lower redshift galaxy overlaps with the observed photometry of the higher redshift galaxy. Given the redshifts of these objects and our data driven approach, our K -corrected magnitudes cannot significantly deviate from the observed photometry, which allows us to K -correct even low signal-to-noise bands like W3 and W4.

NASA Galaxy Evolution Explorer. GALEX is operated for NASA by the California Institute of Technology under NASA contract NAS5-98034.

This publication makes use of data products from SDSS-IV. Funding for the Sloan Digital Sky Survey IV has been provided by the Alfred P. Sloan Foundation, the U.S. Department of Energy Office of Science, and the Participating Institutions.

SDSS-IV acknowledges support and resources from the Center for High Performance Computing at the University of Utah. The SDSS website is www.sdss.org.

SDSS-IV is managed by the Astrophysical Research Consortium for the Participating Institutions of the SDSS Collaboration including the Brazilian Participation Group, the Carnegie Institution for Science, Carnegie Mellon University, Center for Astrophysics | Harvard & Smithsonian, the Chilean Participation Group, the French Participation Group, Instituto de Astrofísica de Canarias, The Johns Hopkins University, Kavli Institute for the Physics and Mathematics of the Universe (IPMU) / University of Tokyo, the Korean Participation Group, Lawrence Berkeley National Laboratory, Leibniz Institut für Astrophysik Potsdam (AIP), Max-Planck-Institut für Astronomie (MPIA Heidelberg), Max-Planck-Institut für Astrophysik (MPA Garching), Max-Planck-Institut für Extraterrestrische Physik (MPE), National Astronomical Observatories of China, New Mexico State University, New York University, University of Notre Dame, Observatório Nacional / MCTI, The Ohio State University, Pennsylvania State University, Shanghai Astronomical Observatory, United

Kingdom Participation Group, Universidad Nacional Autónoma de México, University of Arizona, University of Colorado Boulder, University of Oxford, University of Portsmouth, University of Utah, University of Virginia, University of Washington, University of Wisconsin, Vanderbilt University, and Yale University.

This publication makes use of data products from the Two Micron All Sky Survey, which is a joint project of the University of Massachusetts and the Infrared Processing and Analysis Center/California Institute of Technology, funded by the National Aeronautics and Space Administration and the National Science Foundation.

This publication makes use of data products from the Wide-field Infrared Survey Explorer, which is a joint project of the University of California, Los Angeles, and the Jet Propulsion Laboratory/California Institute of Technology, funded by the National Aeronautics and Space Administration.

DATA AVAILABILITY

Data used in this article is provided publicly at the GSWLC website. The reduced data used in this article is provided publicly on our project GitHub. The ReadMe also provides a detailed description of the data products. Additional data is available upon request.

REFERENCES

- Ahn C. P., et al., 2014, *ApJS*, **211**, 17
- Akaike H., 1974, in *A new look at the statistical model identification*. pp AC–19(6):716–723
- Beare R., Brown M. J. I., Pimblett K., 2014, *ApJ*, **797**, 104
- Bell E. F., et al., 2004, *ApJ*, **608**, 752
- Blanton M. R., Roweis S., 2007, *AJ*, **133**, 734
- Blanton M. R., et al., 2003, *AJ*, **125**, 2348
- Boquien M., Burgarella D., Roehlly Y., Buat V., Ciesla L., Corre D., Inoue A. K., Salas H., 2019, *A&A*, **622**, A103
- Brinchmann J., Charlot S., White S. D. M., Tremonti C., Kauffmann G., Heckman T., Brinkmann J., 2004, *MNRAS*, **351**, 1151
- Brown M. J. I., Dey A., Jannuzi B. T., Brand K., Benson A. J., Brodwin M., Croton D. J., Eisenhardt P. R., 2007, *ApJ*, **654**, 858
- Brown M. J. I., et al., 2014, *ApJS*, **212**, 18
- Bruzual G., Charlot S., 2003, *MNRAS*, **344**, 1000
- Chilingarian I. V., Melchior A.-L., Zolotukhin I. Y., 2010, *MNRAS*, **405**, 1409
- Coleman G. D., Wu C. C., Weedman D. W., 1980, *ApJS*, **43**, 393
- Connolly A. J., Szalay A. S., Bershadsky M. A., Kinney A. L., Calzetti D., 1995, *AJ*, **110**, 1071
- Conroy C., 2013, *ARA&A*, **51**, 393
- Efron B., 1979, *The Annals of Statistics*, **7**, 1
- Fielder C. E., Newman J. A., Andrews B. H., Zasowski G., Boardman N. F., Licquia T., Masters K. L., Salim S., 2021, arXiv e-prints, p. [arXiv:2106.14900](https://arxiv.org/abs/2106.14900)
- Fioc M., Rocca-Volmerange B., 1997, *A&A*, **500**, 507
- Hogg D. W., Baldry I. K., Blanton M. R., Eisenstein D. J., 2002, arXiv e-prints, [pp astro-ph/0210394](https://arxiv.org/abs/astro-ph/0210394)
- Huber P. J., 1964, *Annals of Mathematical Statistics*, **35**, 73–101
- Humason M. L., Mayall N. U., Sandage A. R., 1956, *AJ*, **61**, 97
- Hunter J. D., 2007, *Computing in Science Engineering*, **9**, 90
- Kauffmann G., et al., 2003, *MNRAS*, **341**, 33
- Kewley L. J., Dopita M. A., Sutherland R. S., Heisler C. A., Trevena J., 2001, *ApJ*, **556**, 121
- Kinney A. L., Calzetti D., Bohlin R. C., McQuade K., Storchi-Bergmann T., Schmitt H. R., 1996, *ApJ*, **467**, 38
- Lang D., Hogg D. W., Schlegel D. J., 2016, *AJ*, **151**, 36
- Licquia T. C., Newman J. A., Brinchmann J., 2015, *ApJ*, **809**, 96
- Madgwick D. S., Somerville R., Lahav O., Ellis R., 2003a, *MNRAS*, **343**, 871
- Madgwick D. S., et al., 2003b, *ApJ*, **599**, 997
- Magris C. G., Mateu P. J., Mateu C., Bruzual A. G., Cabrera-Ziri I., Mejía-Narváez A., 2015, *PASP*, **127**, 16
- Maindonald J. W., Braun J., 2010, *Data Analysis and Graphics Using R: An Example-Based Approach*, 3rd Edition. Cambridge University Press
- Maraston C., 2005, *MNRAS*, **362**, 799
- Martin C., GALEX Team 2005, in Colless M., Staveley-Smith L., Stathakis R. A., eds, Vol. 216, *Maps of the Cosmos*. p. 221, [doi:10.1017/S0074180900196664](https://doi.org/10.1017/S0074180900196664)
- McKinney W., 2010, in Stéfan van der Walt Jarrod Millman eds, *Proceedings of the 9th Python in Science Conference*. SciPy, pp 56 – 61, [doi:10.25080/Majora-92bf1922-00a](https://doi.org/10.25080/Majora-92bf1922-00a)
- Newman J. A., et al., 2013, *ApJS*, **208**, 5
- O’Mill A. L., Duplancic F., García Lambas D., Sodré Laerte J., 2011, *MNRAS*, **413**, 1395
- Oke J. B., Sandage A., 1968, *ApJ*, **154**, 21
- Pedregosa F., et al., 2011, *Journal of Machine Learning Research*, **12**, 2825
- Perez F., Granger B. E., 2007, *Computing in Science Engineering*, **9**, 21
- Salim S., et al., 2007, *ApJS*, **173**, 267
- Salim S., et al., 2016, *ApJS*, **227**, 2
- Salim S., Boquien M., Lee J. C., 2018, *ApJ*, **859**, 11
- Skrutskie M. F., et al., 2006, *AJ*, **131**, 1163
- Tremonti C. A., et al., 2004, *ApJ*, **613**, 898
- Uzeirbegovic E., Martin G., Kaviraj S., 2022, *MNRAS*, **510**, 3849
- Virtanen P., et al., 2020, *Nature Methods*,
- Westra E., Geller M. J., Kurtz M. J., Fabricant D. G., Dell’Antonio I., 2010, *PASP*, **122**, 1258
- Willmer C. N. A., et al., 2006, *ApJ*, **647**, 853
- Wright E. L., et al., 2010, *AJ*, **140**, 1868
- van der Walt S., Colbert S. C., Varoquaux G., 2011, *Computing in Science Engineering*, **13**, 22

KCORRECT Derived Coefficients			
Passband	med. a_1	b_0	b_1
FUV		-18.557	30.780
NUV		-7.311	13.429
u		2.503	-7.553
g		0.172	-2.849
i		2.609	-2.887
z		1.816	-1.440
J	1.009		
H	1.189		
Ks	3.946		
W1	3.945		
W2	5.520		
W3	6.252		
W4	9.394		

Table A1. Table of $\text{KCORRECT}^0(g-r)$ derived quantities for the median a_1 's, intercept (b_0), and slope (b_1) of the secondary fits for all bands considered in this work. In some cases, information criteria favour simply using the median derived a_1 values, while for others it is preferred to apply the linear relation $a_1 = b_0 + b_1^0(g-r)$. In either case, rest-frame colours can then be determined via the relation $^0(r-Y) = (r-Y)_{\text{obs}} - a_1 z$, where Y is the band for which rest-frame quantities are to be derived.

GSWLC-M2 Derived Coefficients			
Passband	med. a_1	b_0	b_1
FUV		-11.243	19.597
NUV		-4.251	8.790
u		3.986	-9.244
g		1.089	-4.069
i		2.088	-2.089
z	0.777		
J		4.345	-4.506
H		6.955	-7.721
Ks	3.687		
W1	3.548		
W2	5.391		
W3		21.736	-25.185
W4	9.277		

Table A2. As [Table A1](#), but for quantities derived utilising GSWLC-M2 $^0(g-r)$. Note that the set of passbands for which using the median a_1 value was favoured differed in this case.

APPENDIX A: TABLES OF POLYNOMIAL COEFFICIENTS

In this section we present the derived intercept (b_0) and slope (b_1) for the secondary fits described in step (ii) of [Section 2.3](#); these values are sufficient to enable the K -correction to be calculated for any object at low z given its rest-frame $g-r$ colour and redshift. For bands where a constant a_1 is favoured by the information criterion (cf. step (iii) of [Section 2.3](#)), we present the median a_1 value instead (“med. a_1 ”). [Table A1](#) presents results calculated using $\text{KCORRECT}^0(g-r)$ serves as the reference rest-frame colour, while [Table A2](#) presents results where $\text{GSWLC-M2}^0(g-r)$ is used instead. These tables all use the optical SDSS r band as an anchor band; i.e., the K -corrections tabulated are those needed to convert observed $r-Y$ colour, where Y is the band listed in a given row, to rest-frame $r-Y$.

The b_0 and b_1 values in these tables specifically are determined from [Equation 5](#). The reader can use these quantities to determine a_1 for any object given its rest-frame colour. Then by applying [Equation 9](#) one can obtain the rest-frame ($r-Y$) colour for any band Y of interest.

For example, if one wished to determine rest-frame quantities for the optical z -band from these tables, one can determine the a_1 value for an object by applying the relation $a_1 = b_0 + b_1^0(g-r)$, where $^0(g-r)$ is the rest-frame colour of the chosen galaxy. Then one can obtain its for rest-frame colour by calculating $^0(r-z) = (r-z)_{\text{obs}} - a_1 z$. For bands that use median a_1 , the first equation can be bypassed and the median a_1 value used instead. Hence, to determine rest-frame ($r-W4$) colours one can simply compute $^0(r-W4) = (r-W4)_{\text{obs}} - (\text{med. } a_1)z$. If one desires to determine an absolute magnitude rather than a rest-frame colour, this can be determined by next applying [Equation 11](#).

In addition to these tables we provide code for determining med. a_1 , b_0 and b_1 or other related quantities at [our GitHub repository](#). Full public access is provided for adaptation to any other project, under a CC BY-SA 4.0 license.